Nonlinear current and dynamical quantum phase transitions in the flux-quenched Su-Schrieffer-Heeger model

Nonlinear current and dynamical quantum phase transitions in the flux-quenched Su-Schrieffer-Heeger model

Lorenzo Rossi and Fabrizio Dolcini*

Dipartimento di Scienza Applicata e Tecnologia del Politecnico di Torino, I-10129 Torino, Italy

(Received 29 April 2022; accepted 29 June 2022; published 8 July 2022)

We investigate the dynamical effects of a magnetic flux quench in the Su-Schrieffer-Heeger model in a one-dimensional ring geometry. We show that even when the system is initially in the half-filled insulating state, the flux quench induces a time-dependent current that eventually reaches a finite stationary value. Such persistent current, which exists also in the thermodynamic limit, cannot be captured by the linear response theory and is the hallmark of nonlinear dynamical effects occurring in the presence of dimerization. Moreover, we show that for a range of values of dimerization strength and initial flux, the system exhibits dynamical quantum phase transitions, even though the quench is performed within the same topological class of the model.

DOI: 10.1103/PhysRevB.106.045410

I. INTRODUCTION

Many important features of a quantum mechanical system can be gained from the linear response theory (LRT), where the out-of-equilibrium response of the system to a weak perturbation is encoded in a correlation function evaluated at its equilibrium state [1,2]. In particular, LRT is used to establish whether a fermionic system is a conductor or an insulator. Operatively, this can be done through the following gedankenexperiment: We first imagine to switch off all sources of extrinsic scattering phenomena, e.g., with a bath or with disorder. Then, we apply a weak uniform electric pulse $E(t) = \mathcal{E}\delta(t)$ and observe the long-time behavior of the current in the thermodynamic limit. If a finite persistent current eventually flows, the system is a conductor; otherwise, it is an insulator. Explicitly, the LRT current is expressed as $J(t) = (2\pi)^{-1}\mathcal{E}\int d\omega\, \sigma(\omega)e^{-i\omega t}$, and its stationary value $J(+\infty) = D\mathcal{E}$ is determined by the Drude weight D, i.e., the coefficient appearing in the low-frequency singular term of the conductivity [3] $\sigma(\omega) = \sigma_{\rm reg}(\omega) + iD/(\omega + i0^+)$ and characterizing the possibility of a system to sustain ballistic transport. The evaluation of the Drude weight [4] has allowed the identification of interaction-induced insulating states in exactly solvable fermionic models, either by a direct investigation, such as in the Hubbard model [5–7], or indirectly through spin models that can be mapped into fermionic ones through the Jordan-Wigner transformation [8–13]. Moreover, the linear response of systems that are in a stationary out-of-equilibrium state has been investigated [14].

Remarkably, the high control and tunability of cold-atom systems in optical lattices [15,16], together with the ability to realize artificial gauge fields [17,18], intriguingly suggest that the above gedankenexperiment could actually be realized in a quantum quench protocol [19–22]. Consider an isolated fermionic system on a one-dimensional (1D) ring, initially prepared in the ground state of a given Hamiltonian $\hat{H}_i$. Then, suppose that the unitary dynamics is governed by a different final Hamiltonian $\hat{H}_f$, obtained from the previous one by a sudden change in a magnetic flux piercing the ring. Such sudden variation precisely generates the uniform electric pulse mentioned above.

These experimental advances have also spurred interest in the dynamics *beyond* LRT, i.e., when the stationary-state properties of the system are no longer sufficient to describe its dynamical response. In particular, the dynamics resulting from a flux quench has been analyzed in the case of a single-band model of spinless fermions with a homogeneous nearest-neighbor hopping and interaction [23]. Although quantitative discrepancies from the LRT prediction have been numerically found in the gapless phase, the overall qualitative picture relating the existence of a persistent current to a nonvanishing Drude weight seems quite robust.

In this paper, we instead highlight qualitative differences from LRT predictions emerging after a flux quench in a model of spinless fermions hopping in a *dimerized* ring lattice. Specifically, we shall focus on the Su-Schrieffer-Heeger (SSH) model [24,25], recently realized in optical lattices [26–28]. As is well known, such model is gapped even without interactions and, at half filling, describes a two-band (topological) insulator [29,30]. By quenching the initial flux to zero and by analyzing the resulting dynamics, we find two main results. First, while LRT predicts a vanishing Drude weight and a vanishing current [3], the flux quench does lead to a persistent current flowing along the ring, which is thus a signature of nonlinear effects. Second, if the initial flux exceeds a critical value (dependent on the dimerization strength), dynamical quantum phase transitions (DQPTs) [31] occur. Notably, while a quench performed across the two different topological phases of the SSH model is known to give rise to DQPTs [32], the DQPTs we find occur even if the quench is performed within the same topological phase.

*fabrizio.dolcini@polito.it

We emphasize that the effects predicted here are intrinsically ascribed to the dimerization and arise even without interaction, in sharp contrast to the customary single-band tight-binding model with homogeneous hopping, where interaction is needed to observe any nontrivial dynamical effect of the flux quench [23]. Here, dimerization provides an intrinsically spinorial nature to the Hamiltonian and to its eigenstates, implying that the current operator is not a constant of motion even without interaction. Furthermore, in the single-band model the eigenstates of the Hamiltonian are uniquely determined by their (quasi)momenta and do not depend on the flux, while in the dimerized case the eigenstates exhibit a nontrivial dependence on the flux. Finally, it is the spinorial nature, which is thus absent in the single-band tight-binding model, that leads to the DQPTs.

Our paper is organized as follows. In Sec. II, we present the model and describe the flux-quench dynamics of a two-band model. In Sec. III, we derive the expression of the persistent current and show that while in the limit of vanishing dimerization the LRT captures the metallic behavior, in the presence of dimerization the persistent current flows even though the LRT predicts a vanishing Drude weight and an insulating behavior. In Sec. IV, we then analyze the DQPTs induced by the dimerization. Finally, in Sec. V, we discuss our results and draw our conclusions.

II. MODEL AND STATE EVOLUTION

A. The SSH model

As mentioned in Sec. I, in this article we focus on a well-known example of a band insulator, namely, the Su-Schrieffer-Heeger (SSH) model [24,25], in a 1D ring pierced by a magnetic flux. Below, we briefly recall a few aspects of this model that are needed for our analysis. The SSH Hamiltonian in real space is

$$\hat{H}[\phi] = v\sum_{j=1}^{M}(e^{i\phi}\hat{c}^{\dagger}_{jA}\hat{c}_{jB} + re^{i\phi}\hat{c}^{\dagger}_{jB}\hat{c}_{j+1A} + \text{H.c.}) \tag{1}$$

where M denotes the number of cells, containing two sites A and B each, v is a real positive hopping amplitude, $r \geqslant 0$ is the dimerization parameter, and $\hat{c}^{\dagger}_{j\alpha}$ creates a spinless fermion in the site $\alpha = A, B$ of the jth cell. Denoting by Φ the total magnetic flux threading the ring, we adopt the gauge where the phase related to its vector potential [33,34], denoted by ϕ in Eq. (1), is uniform along the ring links, so that $2M\phi = 2\pi(\Phi/\Phi_0)$, where $\Phi_0 = h/e$ is the elementary flux quantum. We are interested in the thermodynamic limit $M \to +\infty$ with a finite flux per unit cell Φ/M.

In Eq. (1), we assume periodic boundary conditions (PBCs), so that the k wave vectors are quantized (also in the presence of flux) as $ka = 2\pi\, n/M$, where $n \in \{-\lfloor M/2\rfloor, \ldots, \lfloor (M-1)/2\rfloor\}$ and a denotes the size of the unit cell. The SSH Hamiltonian is thus rewritten in momentum space as

$$\hat{H}[\phi] = v\sum_{ka=-\pi}^{\pi}(\hat{c}^{\dagger}_{kA}, \hat{c}^{\dagger}_{kB})\,\mathbf{d}(k,\phi)\cdot\boldsymbol{\sigma}\begin{pmatrix}\hat{c}_{kA}\\ \hat{c}_{kB}\end{pmatrix}, \tag{2}$$

where

$$\mathbf{d}(k,\phi) = [\cos\phi + r\cos(ka+\phi), -\sin\phi + r\sin(ka+\phi), 0], \tag{3}$$

and $\boldsymbol{\sigma} = (\sigma_x, \sigma_y, \sigma_z)$ are Pauli matrices acting on the sublattice degree of freedom. The spectrum of single-particle eigenvalues consists of two symmetric energy bands $\varepsilon_{\pm}(k,\phi) = \pm v\epsilon(k,\phi)$, where

$$\epsilon(k,\phi) = \sqrt{1 + r^2 + 2r\cos(ka+2\phi)}. \tag{4}$$

The density matrices of the single-particle eigenstates, in the $\{|kA\rangle, |kB\rangle\}$ basis, are given by

$$\rho_{\pm}(k,\phi) = \tfrac{1}{2}[\sigma_0 \pm \mathbf{u}(k,\phi)\cdot\boldsymbol{\sigma}], \tag{5}$$

where σ_0 is the 2×2 identity matrix, and $\mathbf{u}(k,\phi) = \mathbf{d}(k,\phi)/|\mathbf{d}(k,\phi)|$ is a unit vector.

The SSH model is also known as a prototype model of a topological insulator [29], which exhibits two topologically distinct phases for $r < 1$ and $r > 1$, with $r = 1$ identifying the nondimerized gapless case. Notably, in the presence of a magnetic flux ($\phi \neq 0$), the energy spectrum (4) depends on the wave vector k and on the flux phase ϕ only through the combination $ka + 2\phi$, whereas the Hamiltonian (2) and its eigenstates (5) depend on *both* of these quantities separately. This is due to the dimerization. Indeed, in the limit $r \to 1$ of vanishing dimerization, in the Hamiltonian (2) one has $\mathbf{d}(k,\phi)\cdot\boldsymbol{\sigma} = 2\cos(ka/2 + \phi)[\sigma_x\cos(ka/2) + \sigma_y\sin(ka/2)]$, and the dependence on the flux phase reduces to a mere multiplicative factor. In this case, the single-particle eigenstates become independent of ϕ.

B. State evolution upon a flux quench

Let us suppose that the system is initially prepared in the insulating ground state of the half-filled SSH model with an initial flux phase value ϕ_i, corresponding to a completely filled lower band $\varepsilon_-(k,\phi_i)$. The kth component of the single-particle density matrix at $t = 0$ can thus be written in the $\{|kA\rangle, |kB\rangle\}$ basis as $\rho_i(k) = [\sigma_0 - \mathbf{u}_i(k)\cdot\boldsymbol{\sigma}]/2$, where $\mathbf{u}_i(k) = \mathbf{u}(k,\phi_i)$. Then, the magnetic flux is suddenly switched off and the initial state evolves according to the final Hamiltonian $\hat{H}_f$ characterized in Eq. (2) by $\mathbf{d}_f(k) = \mathbf{d}(k,\phi=0)$, which in turn identifies the unit vector $\mathbf{u}_f(k) = \mathbf{u}(k,\phi=0)$.

Since the k modes do not couple in the quench process, the Liouville–von Neumann equation can be easily integrated and the kth component of the one-body density matrix is uniquely identified, in the $\{|kA\rangle, |kB\rangle\}$ basis, by the time-evolving Bloch vector $\mathbf{u}(k,t)$ through

$$\rho(k,t) = \tfrac{1}{2}[\sigma_0 - \mathbf{u}(k,t)\cdot\boldsymbol{\sigma}]. \tag{6}$$

Specifically, the Bloch vector precesses around the final direction $\mathbf{u}_f(k)$ and can be expressed as the sum of three orthogonal contributions [35],

$$\mathbf{u}(k,t) = \mathbf{d}_{\parallel}(k) + \mathbf{d}_{\perp}(k)\cos\left[\frac{2\epsilon(k,0)vt}{\hbar}\right] + \mathbf{d}_{\times}(k)\sin\left[\frac{2\epsilon(k,0)vt}{\hbar}\right], \tag{7}$$

whose explicit expressions can be deduced from the general state evolution in a two-band model (see Appendix A 1) and read

$$\mathbf{d}_{\parallel}(k) = d_{\parallel}(k,\phi_i)\mathbf{u}_f(k), \tag{8}$$

$$\mathbf{d}_{\perp}(k) = d_{\perp}(k,\phi_i)\mathbf{R}_z[\mathbf{u}_f(k)], \tag{9}$$

$$\mathbf{d}_{\times}(k) = d_{\perp}(k,\phi_i)(-\mathbf{e}_z). \tag{10}$$

Here,

$$\mathbf{R}_z = \begin{pmatrix} 0 & 1 & 0 \\ -1 & 0 & 0 \\ 0 & 0 & 1 \end{pmatrix} \tag{11}$$

is a matrix describing a rotation by $-\pi/2$ around the z axis identified by the unit vector $\mathbf{e}_z$ and orthogonal to the $\mathbf{d}_i$-$\mathbf{d}_f$ plane, while

$$d_{\parallel}(k,\phi_i) = \frac{(1+r^2)\cos\phi_i + 2r\cos(ka+\phi_i)}{\epsilon(k,\phi_i)\epsilon(k,0)}, \tag{12}$$

$$d_{\perp}(k,\phi_i) = \frac{(1-r^2)\sin\phi_i}{\epsilon(k,\phi_i)\epsilon(k,0)}. \tag{13}$$

As a last remark, we notice that in the limit $r \to 1$ of vanishing dimerization, the dynamics in Eq. (7) becomes trivial since $d_{\perp}(k,\phi_i) = 0$ and $d_{\parallel}(k,\phi) = \mathrm{sign}[\cos(ka/2+\phi_i)\cos(ka/2)]$. Indeed, without dimerization, the initial state is an eigenstate of $\hat{H}_f$ and its density matrix does not evolve with time.

III. CURRENT

Let us now investigate the dynamical behavior of the particle current generated by the quench. We first note that because the system is bipartite, there actually exist two types of currents, namely, intercell and intracell current operators. Their explicit expression straightforwardly stems from the continuity equation related to the postquench Hamiltonian $\hat{H}_f$ (see Appendix A 2) and reads

$$\hat{J}_j^{\mathrm{inter}} = \frac{rv}{\hbar}[i\hat{c}_{jB}^{\dagger}\hat{c}_{j+1A} - i\hat{c}_{j+1A}^{\dagger}\hat{c}_{jB}], \tag{14}$$

$$\hat{J}_j^{\mathrm{intra}} = \frac{v}{\hbar}[i\hat{c}_{jA}^{\dagger}\hat{c}_{jB} - i\hat{c}_{jB}^{\dagger}\hat{c}_{jA}]. \tag{15}$$

Note that since $\hat{H}_f$ has a vanishing flux, these operators do not explicitly depend on the flux. Due to the translational invariance of both the initial state and the final Hamiltonian, the expectation values of Eqs.(14) and (15) are actually independent of the specific cell label j. It is thus worth introducing the space-averaged operators $\hat{J}^l \equiv M^{-1}\sum_{j=1}^{M}\hat{J}_j^l$ (with $l = \mathrm{inter/intra}$), obtaining

$$\hat{J}^l = \frac{1}{M}\sum_{ka=-\pi}^{\pi}(\hat{c}_{kA}^{\dagger},\hat{c}_{kB}^{\dagger})\,\mathcal{J}_k^l\begin{pmatrix}\hat{c}_{kA}\\ \hat{c}_{kB}\end{pmatrix}, \tag{16}$$

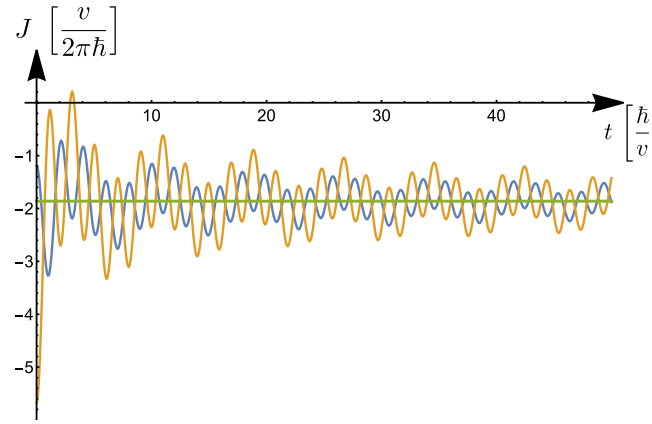

FIG. 1. The intercell current J^{inter} (blue curve) and the intracell current J^{intra} (yellow curve) resulting from a sudden flux quench in the SSH model are plotted as a function of time. At long time, they both tend to the same stationary contribution J_{dc} (green curve). The time evolution is computed in the thermodynamic limit for $r = 0.6$ and $\phi_i = \pi/2$.

where

$$\mathcal{J}_k^{\mathrm{inter}} = \frac{rv}{\hbar}[-\sin(ka)\sigma_x + \cos(ka)\sigma_y], \tag{17}$$

$$\mathcal{J}_k^{\mathrm{intra}} = -\frac{v}{\hbar}\sigma_y. \tag{18}$$

Their expectation values $J^l(t) \equiv \langle\hat{J}^l\rangle(t) = M^{-1}\sum_k \mathrm{tr}[\mathcal{J}_k^l\rho(k,t)]$ for $t > 0$ can be written as

$$J^l(t) = J_{\mathrm{dc}} + J_{\mathrm{ac}}^l(t), \quad l = \mathrm{inter/intra}, \tag{19}$$

where the first term J_{dc} describes a steady-state contribution and is thus the same for inter/intra contributions, while the second term describes the time-dependent fluctuations around it and is different in the two contributions. Explicitly, the ac terms read

$$J_{\mathrm{ac}}^{\mathrm{inter}}(t) = \frac{rv}{\hbar}\frac{1}{M}\sum_{ka=-\pi}^{\pi} d_{\perp}(k,\phi_i)\frac{r+\cos(ka)}{\epsilon(k,0)} \times \cos\left[\frac{2\epsilon(k,0)vt}{\hbar}\right] \tag{20}$$

and

$$J_{\mathrm{ac}}^{\mathrm{intra}}(t) = -\frac{v}{\hbar}\frac{1}{M}\sum_{ka=-\pi}^{\pi} d_{\perp}(k,\phi_i)\frac{1+r\cos(ka)}{\epsilon(k,0)} \times \cos\left[\frac{2\epsilon(k,0)vt}{\hbar}\right], \tag{21}$$

whereas the dc current is

$$J_{\mathrm{dc}} = \frac{rv}{\hbar}\frac{1}{M}\sum_{ka=-\pi}^{\pi} d_{\parallel}(k,\phi_i)\,\frac{\sin(ka)}{\epsilon(k,0)}, \tag{22}$$

with $d_{\parallel}(ka,\phi_i)$ and $d_{\perp}(ka,\phi_i)$ given by Eqs.(12) and (13). Figure 1 displays the time evolution of $J^{\mathrm{intra}}(t)$ and $J^{\mathrm{inter}}(t)$ in the thermodynamic limit $M^{-1}\sum_k \to (2\pi)^{-1}\int d(ka)$. As one can see, the two currents are, in general, different and exhibit long-living fluctuations, described by the ac terms in Eq. (19). However, these fluctuations eventually vanish and

both currents converge to the same steady-state contribution $J_{\rm dc}$, highlighted by the green line.

A few comments are in order about such persistent current $J_{\rm dc}$. First, $J_{\rm dc}$ is essentially different from the current flowing at equilibrium in a mesoscopic ring threaded by a flux, since it is also nonvanishing in the thermodynamic limit, where it acquires the form

$$J_{\rm dc} = \frac{v}{2\pi\hbar}\int_{-\pi}^{\pi} d(ka)\,\frac{r\sin(ka)}{\epsilon(k,0)} \times \frac{(1+r^2)\cos\phi_i + 2r\cos(ka+\phi_i)}{\epsilon(k,\phi_i)\epsilon(k,0)}. \tag{23}$$

Second, $J_{\rm dc}$ cannot be captured by the LRT, which would predict a vanishing persistent current due to a vanishing Drude weight (see Appendix A 3). This can also be seen by inspecting Eq. (23) in the limit of weak initial flux $\phi_i \ll 1$, which corresponds to the limit of weak applied electric pulse. Indeed, one obtains

$$J_{\rm dc} \approx -\frac{v\,r^2}{\pi\hbar}(1-r^2)^2\left[\int_{-\pi}^{\pi} d(ka)\frac{\sin^2(ka)}{\epsilon^7(k,0)}\right]\phi_i^3, \tag{24}$$

which highlights the nonlinear (cubic) response of the insulating SSH ring.

It is now worth comparing the above results with the one of the nondimerized limit $r \to 1$, where one obtains, for the postquench currents ($t > 0$),

$$J^{\rm inter}(t) = J^{\rm intra}(t) = -\frac{2v}{\pi\hbar}\sin\phi_i. \tag{25}$$

Differently from the result obtained for the dimerized case (see Fig. 1), the current (25) is time independent after the quench [36] and, for a weak field $\phi_i \ll 1$, it exhibits a linear dependence on ϕ_i. One thus recovers the well-known finite Drude weight [37] $D = -(e^2/\hbar)\mathrm{v}_F/\pi$, where v_F is the Fermi velocity, of a noninteracting half-filled metallic band, as predicted by LRT [38].

The role of dimerization is emphasized in Fig. 2, where the persistent current (23) is depicted as a function of the initial flux, for various values of dimerization r. While at small flux values $\phi_i \ll 1$ the current $J_{\rm dc}$ of the dimerized case $r \neq 1$ is suppressed as compared to the metallic case $r = 1$ (green curve), for finite flux values the two cases exhibit comparable currents.

The origin of the persistent current term $J_{\rm dc}$ can be understood in terms of the out-of-equilibrium occupancies $n_{f,\pm}$ of the postquench bands $\varepsilon_\pm(k,0)$ induced by the flux quench. These can be computed, for each k, by projecting the initial state on the postquench eigenmodes, obtaining time-independent expressions:

$$\begin{aligned} n_{f,\pm}(k,\phi_i) &= \mathrm{tr}\{\rho_i(k)[\sigma_0 \pm \mathbf{u}_f(k)\cdot\boldsymbol{\sigma}]/2\} \\ &= \frac{1}{2}[1 \mp \mathbf{u}_i(k)\cdot\mathbf{u}_f(k)] \\ &= \frac{1}{2} \mp \frac{(1+r^2)\cos\phi_i + 2r\cos(ka+\phi_i)}{2\epsilon(k,\phi_i)\epsilon(k,0)}, \end{aligned} \tag{26}$$

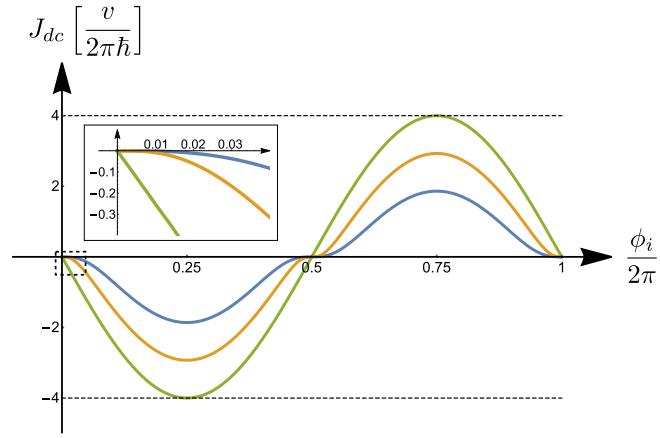

FIG. 2. The persistent current $J_{\rm dc}$ induced in the SSH model by quenching the flux to zero as a function of the initial flux ϕ_i. The blue, yellow, and green curves are obtained for different dimerization strengths, namely, $r = (0.6, 0.8, 1)$, respectively. For each value of $r \neq 1$, the current does not exhibit a linear term in ϕ_i for $\phi_i \ll 1$. The inset magnifies the behavior at small fluxes to highlight the difference between the linear and nonlinear responses.

which are plotted as a function of ka/π in Fig. 3. By comparing Eq. (26) with Eq. (23), the persistent current can be rewritten as

$$J_{\rm dc} = \frac{1}{2\pi a}\int_{-\pi}^{\pi} d(ka)\,\Delta n_f(k,\phi_i)\,\frac{1}{\hbar}\partial_k\varepsilon_-(ka), \tag{27}$$

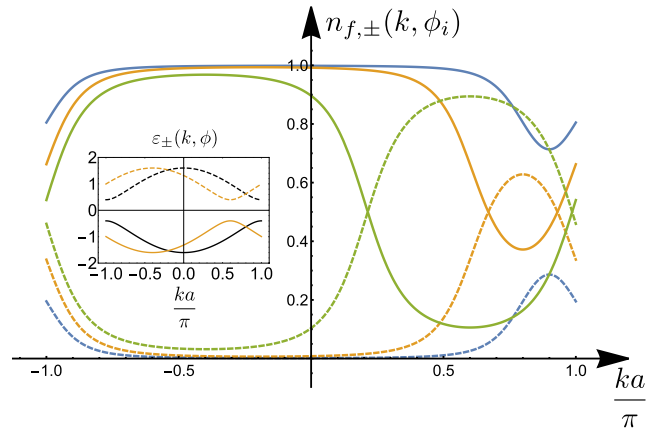

FIG. 3. Occupancies of the postquench bands for different values of the initial flux ϕ_i and a fixed dimerization strength $r = 0.6$. Dashed lines correspond to the upper band, while solid lines correspond to the lower one. The blue, yellow, and green colors correspond to $\phi_i = (0.1, 0.2, 0.4)\pi$, respectively. The distributions are not symmetric in $k \leftrightarrow -k$ for any value of the initial flux. As ϕ_i is increased, the upper band becomes more occupied and the lower band gets more depleted. Inset: bands $\varepsilon_\pm(k,\phi)$ of a SSH model pierced by a magnetic flux. Solid and dashed lines describe the lower and the upper bands, respectively. The bands are depicted for $v = 1$, a fixed dimerization strength $r = 0.6$, and for two different values of the flux, namely, $\phi = 0.2\pi$ (yellow lines) and $\phi = 0$ (black lines).

where $\frac{1}{\hbar}\partial_k \varepsilon_\pm(k) = \pm\frac{va}{\hbar}\frac{r\sin(ka)}{\epsilon(ka)}$ are the postquench group velocities, and

$$\Delta n_f(k,\phi_i) = n_{f,-}(k,\phi_i) - n_{f,+}(k,\phi_i) = \mathbf{u}_i(k)\cdot\mathbf{u}_f(k) \quad (28)$$

denotes the occupancy difference. Since in Eq. (27) the group velocities are odd functions in k, the origin of the nonvanishing persistent current $J_{\rm dc}$ boils down to the lack of even parity in k of the postquench occupancy distributions (26) and of their difference Δn_f. Such lack of symmetry, clearly seen in Fig. 3, arises from the fact that the flux quench impacts the *phase* of the tunneling amplitudes, whereas quenches in the magnitude of the tunneling amplitudes lead to out-of-equilibrium occupancy distributions that preserve their even parity in k and cannot induce a net current [39].

We conclude this section with two comments. First, when moving away from half filling, the system becomes metallic even in the presence of dimerization. In this case, one can show that the system develops a finite Drude weight and that the linear response theory well captures the quench-induced current for small initial fluxes. Nonetheless, there exist some qualitative differences with respect to the nondimerized metallic case. Indeed, because of dimerization, the current also has a finite ac contribution and, for small filling, it does not increase monotonically in $\phi_i \in [0,\pi/2]$, developing a local minimum for $\phi_i = \pi/2$ instead of a maximum. The second comment is concerned with the flux switching protocol. Here, in analogy to what was done in Ref. [23], we have considered the switching off of the initial flux, so that the latter only appears in the initial state. In the reversed protocol, where the flux is switched on, one obtains a current with opposite sign, as expected, provided that one consistently includes the flux phases related to the vector potential both in the postquench Hamiltonian and in the current operators (14) and (15).

IV. DYNAMICAL QUANTUM PHASE TRANSITIONS

Let us now analyze the properties of the Loschmidt amplitude $\mathcal{G}(t) = \langle\psi_0|e^{-i\hat{H}_f t/\hbar}|\psi_0\rangle$, where $|\psi_0\rangle$ is the many-body initial state, while $\hat{H}_f$ is the final Hamiltonian that governs the time evolution of the system after the quench. With applications in studies on quantum chaos and dephasing [40–42], the Loschmidt amplitude has a tight relation to the statistics of the work performed through the quench [31,43,44]. Equivalently, it can also be regarded as the generating function of the energy probability distribution encoded in the postquench diagonal ensemble, since $\mathcal{G}(t) = \int dE P(E) e^{-iEt/\hbar}$, and the postquench diagonal ensemble is described by $P(E) = \sum_n |\langle n|\psi_0\rangle|^2 \delta(E - E_n)$, where E_n and $|n\rangle$ are the many-body eigenvalues and eigenstates of the final Hamiltonian, respectively. Moreover, it has been suggested [31] that the Loschmidt amplitude can be interpreted as a dynamical partition function whose zeros, in analogy with the equilibrium case, are identified with DQPTs. The initial belief of a connection between DQPTs and quenches across different equilibrium phase transitions has been proved to be not rigorous [45–50], and the impact of DQPTs on local observables has been found only in specific cases [31,51–55]. Nevertheless, the existence of zeros of $\mathcal{G}(t)$ can be interpreted as a clear signature of quench-induced population inversion [31,56].

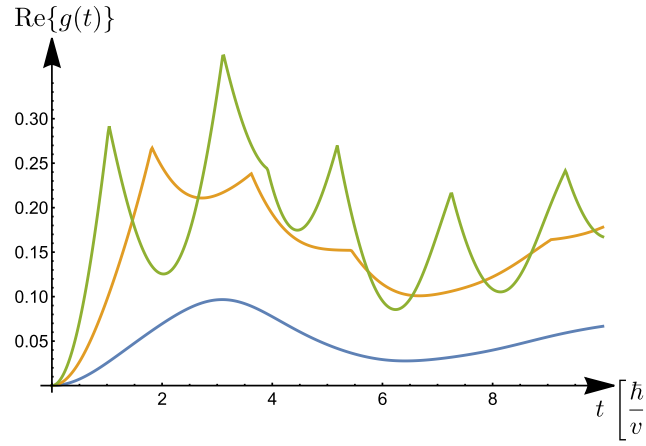

FIG. 4. Time evolution of the real part of the dynamical free-energy density $g(t)$, for different values of the initial flux ϕ_i at a fixed dimerization strength $r = 0.6$. The blue curve corresponds to an initial flux $\phi_i = 0.1\pi$ lying outside the range identified by Eq. (31) and is smooth. The yellow and green curves correspond to flux values that fulfill Eq. (31) [$\phi_i = (0.2, 0.4)\pi$, respectively] and exhibit DQPT singularities.

For the present flux quench, the Loschmidt amplitude explicitly reads [32]

$$\mathcal{G}(t) = \prod_{-\pi\leqslant ka\leqslant\pi}\left[\cos\left(\frac{\epsilon(k,0)vt}{\hbar}\right) + i[\mathbf{u}_i(k)\cdot\mathbf{u}_f(k)]\sin\left(\frac{\epsilon(k,0)vt}{\hbar}\right)\right], \quad (29)$$

where the dynamical free-energy density $g(t) = -M^{-1}\ln[\mathcal{G}(t)]$ in the thermodynamic limit is straightforwardly given by

$$g(t) = -\frac{1}{2\pi}\int_{-\pi}^{\pi} d(ka)\ln\left[\cos\left(\frac{\epsilon(k,0)vt}{\hbar}\right) + i[\mathbf{u}_i(k)\cdot\mathbf{u}_f(k)]\sin\left(\frac{\epsilon(k,0)vt}{\hbar}\right)\right]. \quad (30)$$

The argument of the logarithm in Eq. (30) may vanish at some critical times if and only if $\mathbf{u}_i(k)\cdot\mathbf{u}_f(k) = 0$. Using Eqs. (28) and (26) in the regime $r \neq 1$, this condition can be satisfied by some $ka \in [-\pi,\pi]$ if and only if

$$|\cos\phi_i| \leqslant \frac{2r}{1+r^2}. \quad (31)$$

In conclusion, for each value of the dimerization strength $r \neq 1$, there exists a range of initial flux values, given by Eq. (31), such that singularities in the dynamical free-energy density appear, as shown in Fig. 4. Recalling Eq. (28), we observe that DQPTs appear if and only if the postquench band occupancies cross at some k, i.e., if there exists a subregion of the Brillouin zone where the postquench upper band is more populated then the lower one (band population inversion). This is the case for the yellow and green curves in Figs. 3 and 4. Notably, while a quench across the critical point $r = 1$ is sufficient to induce

a DQPT [32], it is not a necessary condition and *accidental* DQPTs can also appear [45,49]. This is the case here, where the DQPTs show up even if the quench is performed within the same topological phase.

Before concluding this section, a remark is in order about the specific case $r = 1$, which deserves some care. At first, by looking at the limit $r \to 1$ of Eq. (31), one could naively expect that DQPTs exist for any value of the initial flux. However, this is not the case since the scalar product $\mathbf{u}_i(k) \cdot \mathbf{u}_f(k)$ reduces to a pure sign and the argument of the logarithm in Eq. (30) can never vanish. Indeed, for $r = 1$, the initial state is an (excited) eigenstate of the final Hamiltonian, its dynamics is trivial, and $\mathcal{G}(t)$ reduces to a pure oscillating phase [44]. Hence the Loschmidt amplitude can never vanish and the dynamical free-energy density is analytic for $t > 0$. Moreover, for $r = 1$, a description in terms of a two-band structure is redundant and a proper band population inversion cannot be defined without ambiguities.

V. DISCUSSION AND CONCLUSIONS

Our results have been obtained in the case of a sudden flux quench. Here we would like to briefly discuss the effects of a finite switch-off time $\tau_{\rm sw}$. By implementing a time-dependent flux phase $\phi(t) = \phi_i[1 - \mathrm{Erf}(\sqrt{8}t/\tau_{\rm sw})]$ and by numerically integrating the Liouville–von Neumann equation for the density matrix, one can show that the persistent current $J_{\rm dc}$ depends on the ratio $\tau_{\rm sw}/\tau_g$, where $\tau_g = \hbar/(2v|1 - r|)$ is the timescale associated to the energy gap of the SSH model. In particular, while for $\tau_{\rm sw} \ll \tau_g$ the persistent current $J_{\rm dc}$ is robust, when $\tau_{\rm sw} \simeq \tau_g$ it reduces with respect to the sudden quench value (e.g., to roughly $1/5$ for the parameters of Fig. 1) and it vanishes in the limit $\tau_{\rm sw} \gg \tau_g$ of an adiabatic switch-off. In such limit, a vanishing stationary current is consistent with the recent generalization of LRT to a higher-order response, which predicts that in a band insulator the response to an adiabatic electric field vanishes to all orders in the field strength [57–59].

It is worth pointing out the essential difference between the quench-induced dynamics in an insulating and in a metallic state. For a metallic state, where the response to a weak electric pulse is linear, the persistent current that eventually flows is independent of the quench protocol and is thus fully encoded in the Drude weight. In striking contrast, when a weak field is applied to an insulating state (such as the half-filled SSH model), the response is *nonlinear* and does depend on the quench protocol. Thus, while the vanishing higher-order generalized Drude weights [57,58] only capture the behavior of the system in the adiabatic switching limit, for a sufficiently fast switching a persistent current does flow even in an insulator.

In conclusion, in this paper we have analyzed the response of a half-filled SSH ring to a sudden flux quench or, equivalently, to a sudden pulse of electric field. We have shown that the intrinsically spinorial nature of the problem, due to the dimerization of the hopping amplitudes, induces a nontrivial current dynamics even without interactions. In particular, a time-dependent current flows along the ring and eventually reaches a stationary value, despite the insulating nature of the initial state (see Fig. 1). Such persistent current $J_{\rm dc}$, which depends cubically on a weak initial flux ϕ_i in the presence of dimerization [see Eq. (24) and Fig. 2], is a clear hallmark of a nonlinear dynamics and is ascribed to the peculiar nonequilibrium occupancy induced by the quench (see Fig. 3). For suitable dimerization and flux values, a postquench population inversion occurs, which in turn implies the occurrence of DQPTs (see Fig. 4). Notably, the DQPTs are present even without closing the gap, i.e., when the quench is performed within the same topological phase.

ACKNOWLEDGMENTS

Fruitful discussions with Giuseppe Santoro, Rosario Fazio, Mario Collura, and Alessandro Silva are greatly acknowledged.

APPENDIX

1. State evolution in a quenched two-band system

In this Appendix, we recall the general state evolution after a sudden quench in a two-band model [35]. Let us suppose that the initial state is the half-filled ground state of a two-band Hamiltonian, whose one-body form can be written in momentum space as

$$H_i(k) = v\big[d_i^0(k)\sigma_0 + \mathbf{d}_i(k) \cdot \boldsymbol{\sigma}\big], \tag{A1}$$

where v denotes the reference energy scale. The kth component of the initial state can thus be written as $\rho(k, 0) = [\sigma_0 - \mathbf{u}_i(k) \cdot \boldsymbol{\sigma}]/2$, where $\mathbf{u}_i(k) = \mathbf{d}_i(k)/|\mathbf{d}_i(k)|$. The state evolves according to the postquench Hamiltonian

$$H_f(k) = v\big[d_f^0(k)\sigma_0 + \mathbf{d}_f(k) \cdot \boldsymbol{\sigma}\big], \tag{A2}$$

and, by solving the Liouville–von Neumann equation for the one-body density matrix, one can write the kth component of the time-evolved state as $\rho(k, t) = [\sigma_0 - \mathbf{u}(k, t) \cdot \boldsymbol{\sigma}]/2$, where the time-dependent unit vector can be written as the sum of three orthogonal contributions:

$$\begin{aligned}\mathbf{u}(k, t) = {} & \mathbf{d}_\parallel(k) + \mathbf{d}_\perp(k)\cos[2|\mathbf{d}_f(k)|vt/\hbar] \\ & + \mathbf{d}_\times(k)\sin[2|\mathbf{d}_f(k)|vt/\hbar],\end{aligned} \tag{A3}$$

where

$$\begin{aligned}\mathbf{d}_\parallel(k) &= [\mathbf{u}_i(k) \cdot \mathbf{u}_f(k)]\mathbf{u}_f(k), \\ \mathbf{d}_\perp(k) &= [\mathbf{u}_i(k) - \mathbf{d}_\parallel(k)], \\ \mathbf{d}_\times(k) &= -[\mathbf{u}_i(k) \times \mathbf{u}_f(k)].\end{aligned}$$

Then, by inserting the explicit expression for $\mathbf{d}_i(k)$ and $\mathbf{d}_f(k)$ corresponding to a flux quench in the SSH model [see Eq. (3)], the expressions in Eqs. (8)–(10) are recovered.

2. Current

In this Appendix, we briefly outline how to derive the current operators discussed in Sec. III. Given the site density operators $\hat{n}_{j,\alpha} = \hat{c}^\dagger_{j\alpha}\hat{c}_{j\alpha}$, with $\alpha = A, B$, and the SSH Hamiltonian with $\phi = 0$ [see Eq. (1)], it is straightforward to derive the following Heisenberg equations of motion:

$$\partial_t \hat{n}_{jA} = \hat{J}^{\rm inter}_{j-1} - \hat{J}^{\rm intra}_j, \quad \partial_t \hat{n}_{jB} = \hat{J}^{\rm intra}_j - \hat{J}^{\rm inter}_j,$$

where, by definition,

$$\hat{J}_j^{\text{inter}} = \frac{rv}{\hbar}[i\hat{c}_{jB}^\dagger \hat{c}_{j+1A} - i\hat{c}_{j+1A}^\dagger \hat{c}_{jB}]$$

is the intercell current reported in Eq. (14), while

$$\hat{J}_j^{\text{intra}} = \frac{v}{\hbar}[i\hat{c}_{jA}^\dagger \hat{c}_{jB} - i\hat{c}_{jB}^\dagger \hat{c}_{jA}]$$

is the intracell current reported in Eq. (15).

3. Drude weight

The Drude weight D characterizing the LRT of the SSH model can be computed following Kohn's approach [4]. In particular, in a 1D ring, one has

$$D = -L\frac{d^2E_0(\Phi)}{d^2\Phi}\bigg|_{\Phi=0},$$

where $E_0(\Phi)$ denotes the dependence of the many-body ground-state energy on the magnetic flux Φ threading the ring, while L denotes the ring length. For a tight-binding model, we can associate the magnetic flux Φ to a phase ϕ in the hopping amplitudes according to $N\phi = 2\pi\Phi/\Phi_0$, where N is the number of links in the ring and $\Phi_0 = h/e$ is the magnetic flux quantum. Hence, in a bipartite lattice with two sites per cell, we get

$$\Phi = L\frac{2}{a}\frac{\hbar}{e}\phi, \tag{A4}$$

where a is the lattice constant. Exploiting the linear relation between ϕ and Φ, we can write Kohn's formula as

$$D = -\left(\frac{a}{2}\right)^2\left(\frac{e}{\hbar}\right)^2 L^{-1}\frac{d^2E_0(\phi)}{d^2\phi}\bigg|_{\phi=0}. \tag{A5}$$

Moreover, for translationally invariant one-body Hamiltonians, we can write

$$D = -\left(\frac{a}{2}\right)^2\left(\frac{e}{\hbar}\right)^2 L^{-1}\left[\frac{d^2}{d^2\phi}\sum_{(k,b)\in\mathcal{I}}\varepsilon_b(k,\phi)\right]_{\phi=0},$$

where $\mathcal{I}$ denotes the set of bands b and wave vectors k that are occupied in the many-body ground state without flux, while $\varepsilon_b(k,\phi)$ denotes the band dispersion relations for a finite flux.

Since the single-particle energies depend on the phase ϕ only through the combination $ka + 2\phi$ [see Eq. (4)], the many-body ground-state energy of a half-filled SSH model with dimerization ($r \neq 1$) does not depend on the flux in the thermodynamic limit. Indeed, due to the periodic nature of the lower band over the interval $ka \in [-\pi, \pi]$, one has

$$\begin{aligned} L^{-1}E_0^{r\neq1}(\phi) &= \frac{1}{2\pi}\frac{1}{a}\int_{-\pi}^{\pi} d(ka)\varepsilon_-(k,\phi) \\ &= \frac{1}{2\pi}\frac{1}{a}\int_{-\pi}^{\pi} d(ka)\varepsilon_-(k,0) = L^{-1}E_0^{r\neq1}(0), \end{aligned}$$

and we conclude that the Drude weight (A5) is identically zero in this case, consistent with Eq. (24).

Without dimerization ($r = 1$), the situation is different since we get

$$\begin{aligned} L^{-1}E_0^{r=1}(\phi) &= -\frac{v}{\pi}\frac{2}{a}\int_{-\frac{\pi}{2}}^{\frac{\pi}{2}} d\left(\frac{ka}{2}\right)\cos\left(\frac{ka}{2}+\phi\right) \\ &= -\frac{2v}{\pi}\frac{2}{a}\cos(\phi), \end{aligned}$$

and, from Eq. (A5), one obtains

$$D = -\frac{e^2}{\hbar}\frac{2v}{\hbar\pi}\frac{a}{2} = -\frac{e^2}{\hbar}\frac{\mathrm{v}_F}{\pi},$$

where v_F is the Fermi velocity. The finite Drude weight computed in this way coincides with the one obtained in the main text [see Eq. (25)] through its dynamical definition.

[1] R. Kubo, J. Phys. Soc. Jpn. **12**, 570 (1957).
[2] G. D. Mahan, *Many Particle Physics*, 3rd ed. (Springer, Boston, 2000).
[3] R. Resta, J. Phys.: Condens. Matter **30**, 414001 (2018).
[4] W. Kohn, Phys. Rev. **133**, A171 (1964).
[5] B. S. Shastry and B. Sutherland, Phys. Rev. Lett. **65**, 243 (1990).
[6] N. Kawakami and S.-K. Yang, Phys. Rev. B **44**, 7844 (1991).
[7] H. Castella, X. Zotos, and P. Prelovsek, Phys. Rev. Lett. **74**, 972 (1995).
[8] Zotos, Phys. Rev. Lett. **82**, 1764 (1999).
[9] J. Benz, T. Fukui, A. Klümper, and C. Scheeren, J. Phys. Soc. Jpn. **74**, 181 (2005).
[10] J. Herbrych, P. Prelovšek, and X. Zotos, Phys. Rev. B **84**, 155125 (2011).
[11] C. Karrasch, J. H. Bardarson, and J. E. Moore, Phys. Rev. Lett. **108**, 227206 (2012).
[12] M. Mierzejewski, P. Prelovšek, and T. Prosen, Phys. Rev. Lett. **113**, 020602 (2014).
[13] C. Karrasch, T. Prosen, and F. Heidrich-Meisner, Phys. Rev. B **95**, 060406(R) (2017).
[14] D. Rossini, R. Fazio, V. Giovannetti, and A. Silva, Europhys. Lett. **107**, 30002 (2014).
[15] M. Lewenstein, A. Sanpera, V. Ahufinger, B. Damski, A. Sen, and U. Sen, Adv. Phys. **56**, 243 (2007).
[16] I. Bloch, J. Dalibard, and W. Zwerger, Rev. Mod. Phys. **80**, 885 (2008).
[17] J. Dalibard, F. Gerbier, G. Juzeliunas, and P. Öhberg, Rev. Mod. Phys. **83**, 1523 (2011).
[18] N. Goldman, G. Juzeliūnas, P. Öhberg, and I. B. Spielman, Rep. Prog. Phys. **77**, 126401 (2014).
[19] P. Calabrese and J. Cardy, Phys. Rev. Lett. **96**, 136801 (2006).
[20] A. Polkovnikov, K. Sengupta, A. Silva, and M. Vengalattore, Rev. Mod. Phys. **83**, 863 (2011).
[21] J. Eisert, M. Friesdorf, and C. Gogolin, Nat. Phys. **11**, 124 (2015).
[22] A. Mitra, Annu. Rev. Condens. Matter Phys. **9**, 245 (2018).

[23] Y. O. Nakagawa, G. Misguich, and M. Oshikawa, Phys. Rev. B **93**, 174310 (2016).

[24] W. P. Su, J. R. Schrieffer, and A. J. Heeger, Phys. Rev. Lett. **42**, 1698 (1979).

[25] W. P. Su, J. R. Schrieffer, and A. J. Heeger, Phys. Rev. B **22**, 2099 (1980).

[26] M. Atala, M. Aidelsburger, J. T. Barreiro, D. Abanin, T. Kitagawa, E. Demler, and I. Bloch, Nat. Phys. **9**, 795 (2013).

[27] E. J. Meier, F. A. An, and B. Gadway, Nat. Commun. **7**, 13986 (2016).

[28] D. Xie, W. Gou, T. Xiao, B. Gadway, and B. Yan, npj Quantum Inf. **5**, 55 (2019).

[29] J. K. Asbóth, L. Oroszlány, and A. Pályi, *A Short Course on Topological Insulators* (Springer, Berlin, 2016).

[30] C.-Q. Shen, *Topological Insulators* (Springer, Heidelberg, 2012).

[31] M. Heyl, A. Polkovnikov, and S. Kehrein, Phys. Rev. Lett. **110**, 135704 (2013).

[32] S. Vajna and B. Dora, Phys. Rev. B **91**, 155127 (2015).

[33] R. E. Peierls, Z. Phys. **80**, 763 (1933).

[34] M. Graf and P. Vogl, Phys. Rev. B **51**, 4940 (1995).

[35] C. Yang, L. Li, and S. Chen, Phys. Rev. B **97**, 060304(R) (2018).

[36] The nondimerized limit acquires a time-dependent current only in the presence of interactions; see Ref. [23].

[37] The expression for D is obtained by reexpressing the phase ϕ_i in terms of the initial magnetic flux $\Phi_i = \mathcal{E}_i L$ [see Eq. (A4) in Appendix A 3]. Moreover, an additional factor e has to be included to obtain the charge current from the particle current J in Eq. (25).

[38] T. Giamarchi, *Quantum Physics in One Dimension* (Clarendon Press, Oxford, 2003).

[39] S. Porta, N. T. Ziani, D. M. Kennes, F. M. Gambetta, M. Sassetti, and F. Cavaliere, Phys. Rev. B **98**, 214306 (2018).

[40] R. A. Jalabert and H. M. Pastawski, Phys. Rev. Lett. **86**, 2490 (2001).

[41] Z. P. Karkuszewski, C. Jarzynski, and W. H. Zurek, Phys. Rev. Lett. **89**, 170405 (2002).

[42] H. T. Quan, Z. Song, X. F. Liu, P. Zanardi, and C. P. Sun, Phys. Rev. Lett. **96**, 140604 (2006).

[43] A. Silva, Phys. Rev. Lett. **101**, 120603 (2008).

[44] A. De Luca, Phys. Rev. B **90**, 081403(R) (2014).

[45] S. Vajna and B. Dora, Phys. Rev. B **89**, 161105(R) (2014).

[46] F. Andraschko and J. Sirker, Phys. Rev. B **89**, 125120 (2014).

[47] R. Jafari and H. Johannesson, Phys. Rev. Lett. **118**, 015701 (2017).

[48] R. Jafari, H. Johannesson, A. Langari, and M. A. Martin-Delgado, Phys. Rev. B **99**, 054302 (2019).

[49] L. Pastori, S. Barbarino, and J. C. Budich, Phys. Rev. Research **2**, 033259 (2020).

[50] M. Sadrzadeh, R. Jafari, and A. Langari, Phys. Rev. B **103**, 144305 (2021).

[51] M. Fagotti, arXiv:1308.0277.

[52] J. C. Halimeh and V. Zauner-Stauber, Phys. Rev. B **96**, 134427 (2017).

[53] I. Homrighausen, N. O. Abeling, V. Zauner-Stauber, and J. C. Halimeh, Phys. Rev. B **96**, 104436 (2017).

[54] J. Lang, B. Frank, and J. C. Halimeh, Phys. Rev. B **97**, 174401 (2018).

[55] B. Žunkovič, M. Heyl, M. Knap, and A. Silva, Phys. Rev. Lett. **120**, 130601 (2018).

[56] N. Defenu, T. Enss, and J. C. Halimeh, Phys. Rev. B **100**, 014434 (2019).

[57] H. Watanabe and M. Oshikawa, Phys. Rev. B **102**, 165137 (2020).

[58] H. Watanabe, Y. Liu, and M. Oshikawa, J. Stat. Phys. **181**, 2050 (2020).

[59] R. Resta, arXiv:2111.12617.